

This is the accepted manuscript made available via CHORUS. The article has been published as:

Asymmetry-induced synchronization in oscillator networks

Yuanzhao Zhang, Takashi Nishikawa, and Adilson E. Motter

Phys. Rev. E **95**, 062215 — Published 16 June 2017

DOI: [10.1103/PhysRevE.95.062215](https://doi.org/10.1103/PhysRevE.95.062215)

Asymmetry-Induced Synchronization in Oscillator Networks

Yuanzhao Zhang,¹ Takashi Nishikawa,^{1,2} and Adilson E. Motter^{1,2}

¹*Department of Physics and Astronomy, Northwestern University, Evanston, Illinois 60208, USA*

²*Northwestern Institute on Complex Systems, Northwestern University, Evanston, Illinois 60208, USA*

A scenario has recently been reported in which in order to stabilize complete synchronization of an oscillator network—a symmetric state—the symmetry of the system itself has to be broken by making the oscillators nonidentical. But how often does such behavior—which we term asymmetry-induced synchronization (*AISync*)—occur in oscillator networks? Here we present the first general scheme for constructing *AISync* systems and demonstrate that this behavior is the norm rather than the exception in a wide class of physical systems that can be seen as multilayer networks. Since a symmetric network in complete synchrony is the basic building block of cluster synchronization in more general networks, *AISync* should be common also in facilitating cluster synchronization by breaking the symmetry of the cluster subnetworks.

PACS numbers: 05.45.Xt, 89.75.Fb

I. INTRODUCTION

A common assumption in the field of network dynamics is that homogeneity in the local dynamics [1, 2] and interaction network [3–5]—or in the combination of both [6, 7]—can facilitate complete synchronization. It has been recently shown, however, that structural heterogeneity in networks of identical oscillators [8] or oscillator heterogeneity in structurally symmetric networks [9] can stabilize otherwise unstable synchronous states, thus effectively breaking the symmetry of a system to stabilize a symmetric state. These scenarios, which we refer to as *asymmetry-induced synchronization* (*AISync*), can be interpreted as the converse of symmetry breaking, and hence as a converse of chimera states [10, 11]. Perhaps the most striking and the strongest form of *AISync* is the one in which oscillators coupled in a symmetric network (i.e., each oscillator plays exactly the same structural role) can converge to identical dynamics only when they themselves are nonidentical; this has been demonstrated, however, exclusively for rotationally symmetric networks and one type of periodic oscillators [9]. Whether such *AISync* behavior can be shown to be common among systems with other symmetric network structures and oscillator dynamics, including experimentally testable ones, has been an open question.

In this article we introduce and analyze a broad class of *AISync* systems that can have general symmetric network structure with multiple link types and general oscillator dynamics (which can be chaotic, periodic, continuous-time, discrete-time, etc.). This in particular includes physical systems previously used in network synchronization experiments, thus providing a recipe for future empirical studies. For this class, we demonstrate that *AISync* is indeed common and provide a full characterization of those networks that support *AISync* behavior, showing that the fraction of such networks is significant over a range of network sizes and link densities.

II. DEFINITION OF *AISync*

To formulate a precise definition of *AISync*, we consider networks of N (not necessarily identical) oscillators coupled through K different types of interactions. The network dynamics is described by

$$\dot{\mathbf{X}}_i = \mathbf{F}_i(\mathbf{X}_i) + \sum_{\alpha=1}^K \sum_{\substack{i'=1 \\ i' \neq i}}^N A_{ii'}^{(\alpha)} \mathbf{H}^{(\alpha)}(\mathbf{X}_i, \mathbf{X}_{i'}), \quad (1)$$

where $\mathbf{X}_i = \mathbf{X}_i(t)$ is the M -dimensional state vector of node i , the function \mathbf{F}_i governs the intrinsic dynamics of node i , the (binary) adjacency matrix $A^{(\alpha)} = (A_{ii'}^{(\alpha)})$ represents the topology of interactions through links of type α , and $\mathbf{H}^{(\alpha)}$ is the interaction function associated with the link type α . A completely synchronous state of the network is defined by $\mathbf{X}_1(t) = \mathbf{X}_2(t) = \dots = \mathbf{X}_N(t)$.

To isolate the effect of breaking the homogeneity of oscillators, we consider adjacency matrices $A^{(\alpha)}$ that together represent a *symmetric network*, defined as a network in which every node can be mapped to any other node by some permutation of nodes without changing any $A^{(\alpha)}$. Thus, the set of links of any given type must couple every node identically (see Fig. 1(a) for an example). The rationale for using symmetric network structures here is to ensure that any stabilization of complete synchronization by oscillator heterogeneity is due to the reduced system symmetry (as required for *AISync*) and not due to having network heterogeneity and oscillator heterogeneity compensating each other, which may not break the system symmetry.

When restricted to undirected networks with a single link type, our definition of symmetric networks yields the class of vertex-transitive graphs from graph theory [12]. This rich class encompasses Cayley graphs (defined as a network of relations between elements of a finite group; Appendix A) and circulant graphs (defined as a network whose nodes can be arranged in a ring so that the network is invariant under rotations), which have previously been used to study chimera states [13]. Enumerating

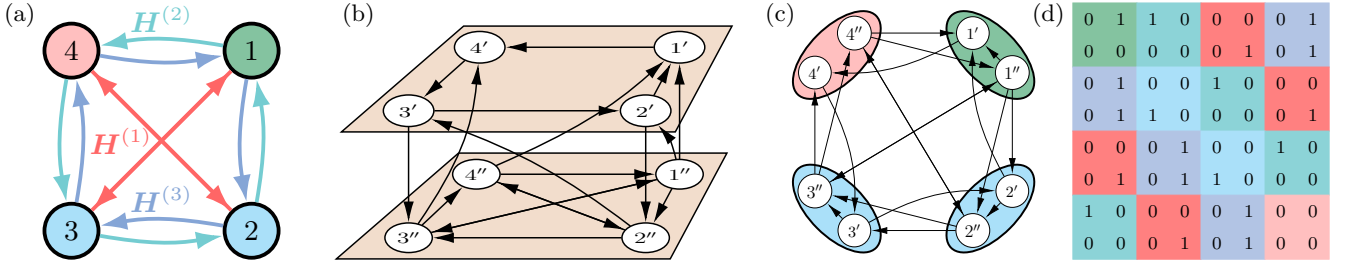


FIG. 1. Multilayer construction of *AISync* networks. (a) Example of a symmetric network of $N = 4$ heterogeneous oscillators and $K = 3$ types of (directed) links with associated interaction functions $H^{(1)}$, $H^{(2)}$ and $H^{(3)}$. (b) One of many possible multilayer networks corresponding to the network in (a), with $L = 2$ layers and $n = LN = 8$ identical subnodes. Subnodes are labeled with node indices, with prime and double prime indicating layer 1 and 2, respectively. (c) Flattened, monolayer representation of the multilayer network in (b). (d) Block structure of the adjacency matrix \tilde{A} for the monolayer network in (c). Colors indicate different types of nodes (diagonal blocks) and links (off-diagonal blocks).

all vertex-transitive graphs of a given size N becomes challenging as N grows and has so far been completed only for $N < 32$ [14]. The symmetric networks we consider here generalizes vertex-transitive graphs to the even richer class of networks that can be directed and include multiple link types.

Given a symmetric network structure, the system in Eq. (1) exhibits *AISync* if it satisfies the following two conditions: (C1) there are no stable synchronous states for any *homogeneous system* (i.e., with $\mathbf{F}_1 = \dots = \mathbf{F}_N$), and (C2) there is a *heterogeneous system* (i.e., with $\mathbf{F}_i \neq \mathbf{F}_{i'}$, for some $i \neq i'$) for which a stable synchronous state exists. A challenge in establishing *AISync* is that the form of Eq. (1) does not guarantee the existence of a completely synchronous state. Another challenge concerns the stability analysis of such a state, since Eq. (1) is beyond the framework normally used in the master stability function (MSF) approach and its generalizations currently available [2, 15–17]: oscillators can be nonidentical (different \mathbf{F}_i), and the network can host $K > 1$ types of directed interactions.

III. MULTILAYER SYSTEMS CONSIDERED

To overcome these challenges, below we propose a *multilayer construction* that defines a large, general subclass of systems within the class given by Eq. (1). We show that any system in this subclass is guaranteed to have a synchronous state, and the stability of that state can be analyzed by applying the MSF framework to the flattened representation of the system. The MSF approach decouples the oscillator dynamics from the network structure, which enables us to draw conclusions about *AISync* for general oscillator dynamics.

In our multilayer system, each node represents a set of L identical *subnodes*, belonging to L different layers and connected by a set of *internal sublinks*. The pattern of these internal sublinks is thus considered part of the node's properties and can be used to represent node het-

erogeneity. For a pair of connected nodes, the type of the connecting link is determined by the pattern of *external sublinks* between the subnodes of these two nodes. This construction yields a multilayer network [18–22] of subnodes and sublinks with L layers; see Fig. 1(b) for an $L = 2$ example. Note that in general there is more than one possible multilayer network for a given symmetric network. Networks with such layered structure have been used extensively as realistic models of various natural and man-made systems. The class of systems just defined is broader than most classes of systems used in previous studies of synchronization on multilayer networks [23, 24], since the links between two different layers are not constrained to be one-to-one. The underlying hierarchical organization, in which each node decomposes into interacting subnodes, is shared by many physical systems, such as the multi-processor nodes in modern supercomputers.

Coupling the dynamics of subnodes diffusively in this network, the multilayer system can be described at the subnode level as

$$\dot{\mathbf{x}}_\ell^{(i)} = \mathbf{f}(\mathbf{x}_\ell^{(i)}) + \sum_{i'=1}^N \sum_{\ell'=1}^L \tilde{A}_{\ell\ell'}^{(ii')} [\mathbf{h}(\mathbf{x}_{\ell'}^{(i')}) - \mathbf{h}(\mathbf{x}_\ell^{(i)})], \quad (2)$$

where $\mathbf{x}_\ell^{(i)} = \mathbf{x}_\ell^{(i)}(t)$ is the m -dimensional state vector for subnode ℓ (i.e., in layer ℓ) of node i , the function \mathbf{f} determines the dynamics of every isolated subnode, and \mathbf{h} is the interaction function common to all sublinks. Here, for all links of a given type between different nodes, the corresponding coupling matrix $\tilde{A}^{(ii')} := (\tilde{A}_{\ell\ell'}^{(ii')})$, $i \neq i'$, is the same and encodes the subnode connection pattern for that link type. In contrast, the subnode connection pattern within each node i is encoded in the matrix $F^{(i)} := (\tilde{A}_{\ell\ell'}^{(ii)})$. Since the subnode-to-subnode interactions are diffusive, the synchronous state given by $\mathbf{x}_\ell^{(i)}(t) = \mathbf{s}(t)$, $\forall i, \ell$ with $\dot{\mathbf{s}} = \mathbf{f}(\mathbf{s})$ is guaranteed to exist. Note that the diffusive couplings among subnodes do not necessarily imply that the node-to-node interactions are diffusive, as intralayer synchronization of the

form $\mathbf{x}_\ell^{(i)} = \mathbf{s}_\ell$ among subnodes is also valid as a state of complete synchronization among all nodes. The interactions among nodes do not vanish in this case due to the existence of external sublink connections among different layers. To summarize, Eq. (2) describes a general class of multilayer models of symmetric networks that admit a state corresponding to complete synchronization, $\mathbf{X}_i(t) = \mathbf{S}(t)$, $\forall i$, when written in the form of Eq. (1) (see Appendix B for details).

IV. ESTABLISHING *AISync*

To facilitate the stability analysis required to establish *AISync*, we flatten the multilayer network representation into a single layer (see Fig. 1(c) for an example). We use $\tilde{A} = (\tilde{A}_{jj'})$ to denote the weighted adjacency matrix that encodes the structure of the resulting monolayer network (see Fig. 1(d) for an example). This matrix has a block structure in which the matrices $F^{(i)}$ appearing on the diagonal blocks characterize node properties, while $\tilde{A}^{(ii')}$ appearing on the off-diagonal blocks reflect the link types. Since subnodes and sublinks are identical, we can directly apply the MSF analysis [25] to the monolayer network and obtain the stability function $\psi(\lambda)$ (see Appendix C for details). The maximum Lyapunov exponent (MLE) of the synchronous state is then computed as $\Psi := \max_{2 \leq j \leq n} \psi(\lambda_j)$, where $\lambda_1, \dots, \lambda_n$ are the eigenvalues of the corresponding Laplacian matrix $\tilde{L} := (\tilde{L}_{jj'})$, defined as $\tilde{L}_{jj'} := \delta_{jj'} \sum_{k=1}^n \tilde{A}_{jk} - \tilde{A}_{jj'}$, where $\delta_{jj'}$ is the Kronecker delta function. Here, λ_1 is the identically zero eigenvalue, which is excluded in the definition of Ψ for corresponding to a mode of perturbation that does not affect synchronization stability. Thus, the synchronous state is asymptotically stable if $\Psi < 0$ and unstable if $\Psi > 0$.

To establish *AISync* for our multilayer system, we first verify that all homogeneous systems have $\Psi > 0$ (i.e., synchronous state $\mathbf{x}_\ell^{(i)} = \mathbf{s}$, $\forall i, \ell$, is unstable), and check numerically that all other synchronous states $\mathbf{x}_\ell^{(i)} = \mathbf{s}_\ell$, $\forall i, \ell$, are also unstable. This establishes condition (C1). We then find a heterogeneous system with $\Psi < 0$, which establishes condition (C2). This procedure is detailed in Appendix D.

In the case of linear \mathbf{f} and \mathbf{h} , which is widely used to study consensus dynamics and encompasses a variety of nontrivial stability regions [26], the problem of verifying *AISync* is fully solvable. To see this, we first note that in this case the stability function $\psi(\lambda)$ determines the (common) stability of *all* completely synchronous states of the form $\mathbf{x}_\ell^{(i)} = \mathbf{s}_\ell$, $\forall i, \ell$, where the subnode states \mathbf{s}_ℓ can in general be different for different ℓ . Next, for a given (homogeneous or heterogeneous) system, we sort its Laplacian eigenvalues into two groups: $\lambda_1, \dots, \lambda_{j^*}$, corresponding only to those perturbations parallel to the synchronization manifold, and $\lambda_{j^*+1}, \dots, \lambda_n$, corresponding to perturbations that are transverse to the man-

ifold and thus destroy synchronization. The stability (of all completely synchronous states) is then determined by $\Psi' := \max_{j^* < j \leq n} \psi(\lambda_j)$, noting that both j^* and λ_j generally depend on the network structure. This leads to the following solution for the *AISync* conditions: $\Psi' \geq 0$ for all homogeneous systems and $\Psi' < 0$ for some heterogeneous system (where we include $\Psi' = 0$ in the first condition because linear systems cannot have asymptotically stable synchronization when $\Psi' = 0$).

V. EXAMPLES OF *AISync*

A. Consensus dynamics

Here we establish *AISync* for the system with the symmetric network structure shown in Fig. 2, in which the subnodes follow the consensus dynamics used in Ref. [26]:

$$\dot{\mathbf{x}}_i = D\mathbf{f}\mathbf{x}_i - \sum_j \tilde{L}_{ij} D\mathbf{h}\mathbf{x}_j, \quad (3)$$

where

$$D\mathbf{f} = \begin{pmatrix} -2 & 2 & -1 & 2 \\ -1 & 1 & 0 & 0 \\ 0 & 0 & -3 & 4 \\ 0 & 0 & -1 & 1 \end{pmatrix} \quad D\mathbf{h} = \begin{pmatrix} 0 & 0 & 0 & 0 \\ 0 & 0 & 0 & 0 \\ 0 & 1 & 0 & -1 \\ -1 & 0 & 1 & 0 \end{pmatrix}. \quad (4)$$

This leads to a stability region $\psi(\lambda) < 0$ shown in Fig. 2(c) defined by

$$x(x+3) - y^2 - (2x+3)^2 y^2 > 0, \quad (5)$$

where x and y denote the real and imaginary parts of λ , respectively.

For $L = 2$ there are only two possible homogeneous systems, associated with the two possible directions of the internal sublink in each node. The homogeneous system in Fig. 2(a) has Laplacian eigenvalues $\lambda_1 = 0$, $\lambda_2 = 2$, $\lambda_{3,4} \approx 0.5 \pm 0.866i$, and $\lambda_{5,6} \approx 1.5 \pm 0.866i$, where λ_1 and λ_2 correspond to the perturbations parallel to the synchronization manifold and $\lambda_3, \dots, \lambda_6$ correspond to those in the transverse directions (i.e., $j^* = 2$). Since $\psi(\lambda_j) > 0$ for $j = 3, 4, 5, 6$ [i.e., all these λ_j 's fall outside the stability region in Eq. (5), as indicated by the red squares in Fig. 2(c)], we have $\Psi' = \max_{2 < j \leq 6} \psi(\lambda_j) > 0$. The other homogeneous system is not synchronizable since all the single-prime subnodes have no incoming sublink. In contrast, for the heterogeneous system in Fig. 2(b), the Laplacian eigenvalues are $\lambda_1 = 0$, $\lambda_j = 1$ for $1 < j \leq 5$, and $\lambda_6 = 2$ (i.e., $j^* = 1$ in this case). As shown by the blue dots in Fig. 2(c), we have $\Psi' = \max_{1 < j \leq 6} \psi(\lambda_j) < 0$ for this heterogeneous system. We thus see that $\Psi' \geq 0$ (i.e., the synchronous state is not asymptotically stable) for both homogeneous systems and $\Psi' < 0$ (i.e., the synchronous state is asymptotically stable) for a heterogeneous system, establishing *AISync*: the agents can reach consensus only when some of them are different from the others.

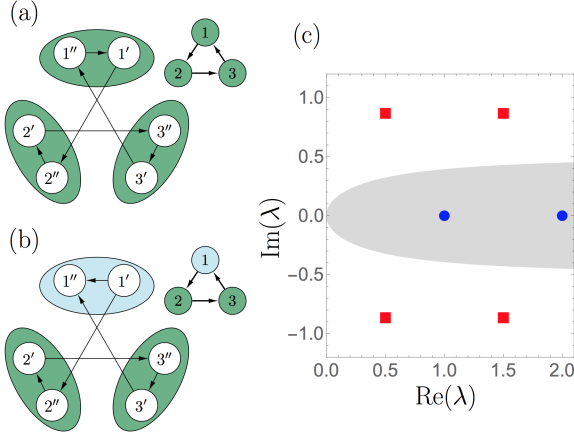


FIG. 2. (Color online) Example of consensus system showing *AISync*. (a) Symmetric network of $N = 3$ homogeneous nodes, each with $L = 2$ subnodes coupled by a directed link (from subnode i'' to i'). (b) The same network but with heterogeneous nodes, in which the direction of the internal sublink in the (light) cyan node is the opposite of that in the (dark) green nodes. In both (a) and (b) we show the corresponding node-level visualization of the network at the top right. (c) Stability region (shaded gray) for the consensus dynamics. All the transverse modes for the homogeneous system in (a) are unstable (red squares), while those for the heterogeneous system in (b) are stable (blue dots).

B. Coupled Lorenz oscillators

An example of nonlinear system exhibiting *AISync* is shown in Fig. 3. The network structure is symmetric and has $N = 3$ nodes and $K = 2$ types of links representing sublink patterns in the clockwise and counterclockwise directions in Fig. 3(a). Each node consists of $L = 2$ subnodes, each of which is a chaotic Lorenz oscillator. The two subnodes are connected by a sublink, the direction of which determines the node type. This gives rise to two node types, and there are four possible distinct combinations of node types for the network—two homogeneous and two heterogeneous. The system has two parameters, a and b , representing the coupling strength of internal and external sublinks, respectively. We seek to determine for which values of a and b the system exhibits *AISync*.

In Fig. 3(b), we show Ψ_+ (red) and Ψ_- (blue) as functions of a and b , where Ψ_+ (Ψ_-) are defined to be the smaller value of Ψ between the two possible homogeneous (heterogeneous) systems. In the region shaded purple (where $\Psi_- > 0$ and $\Psi_+ < 0$), the synchronous state $\mathbf{x}_\ell^{(i)}(t) = \mathbf{s}(t)$, $\forall i, \ell$ is stable for at least one of the heterogeneous systems, but unstable for both homogeneous systems. We further verify in this region that the other possible forms of synchronous states, $\mathbf{x}_\ell^{(i)}(t) = \mathbf{s}_\ell(t)$, $\forall i, \ell$, are unstable for both homogeneous systems (through extensive numerical simulation—see Appendix E for detail). This establishes conditions (C1) and (C2), thus

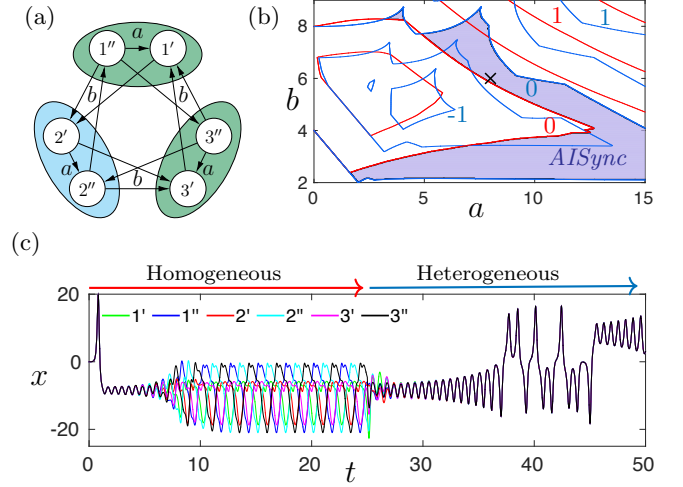


FIG. 3. Example of coupled Lorenz system showing *AISync*. (a) Symmetric network of $N = 3$ nodes, each with $L = 2$ directionally coupled subnodes of Lorenz oscillators. Here we show an instance of a heterogeneous system in which the sublink direction in one node (cyan) is different from the other two (green). (b) Contour plots of Ψ_+ (red) for the case of homogeneous nodes (all-green or all-cyan nodes) and Ψ_- (blue) for heterogeneous nodes (one or two green nodes). The shaded region corresponds to *AISync* systems, for which $\Psi_+ > 0$ and $\Psi_- < 0$. (c) Sample trajectory of the system for $a = 8$ and $b = 6$ [cross symbol in (b)], exhibiting *AISync*. The first component x_1 of the Lorenz oscillator state vector is shown for all $n = 6$ subnodes.

confirming that the system exhibits *AISync* in the purple region. The *AISync* behavior of the system for a specific combination of a and b is illustrated by the sample trajectory in Fig. 3(c), which diverges from synchrony while the nodes are kept homogeneous, but re-synchronizes spontaneously after the nodes are made heterogeneous.

C. Coupled electro-optic systems

We now present an experimentally testable *AISync* system based on the discrete-time model of the electro-optic system implemented in Refs. [16, 27] and given by

$$x_i^{t+1} = \left[f(x_i^t) - \sum_j \tilde{L}_{ij} f(x_j^t) + \delta \right] \bmod 2\pi, \quad (6)$$

where $f(x) = \beta I(x)$ determines the isolated subnode dynamics and also serves as the coupling function. Here, $I(x) = (1 - \cos x)/2$ is the normalized optical intensity, $\beta = 1.7\pi$ is the self-feedback strength, $\delta = 0.2$ is the offset introduced to suppress the trivial solution $x_i = 0$, and \tilde{L}_{ij} is the weighted graph Laplacian [weights controlled by parameters a and b , as shown in Fig. 4(a–c)].

Figure 4 shows an example of *AISync* using these electro-optic maps as subnodes. The internal connections are chosen from the quaternary set (no sublink, one directed sublink in either direction, and directed sublinks

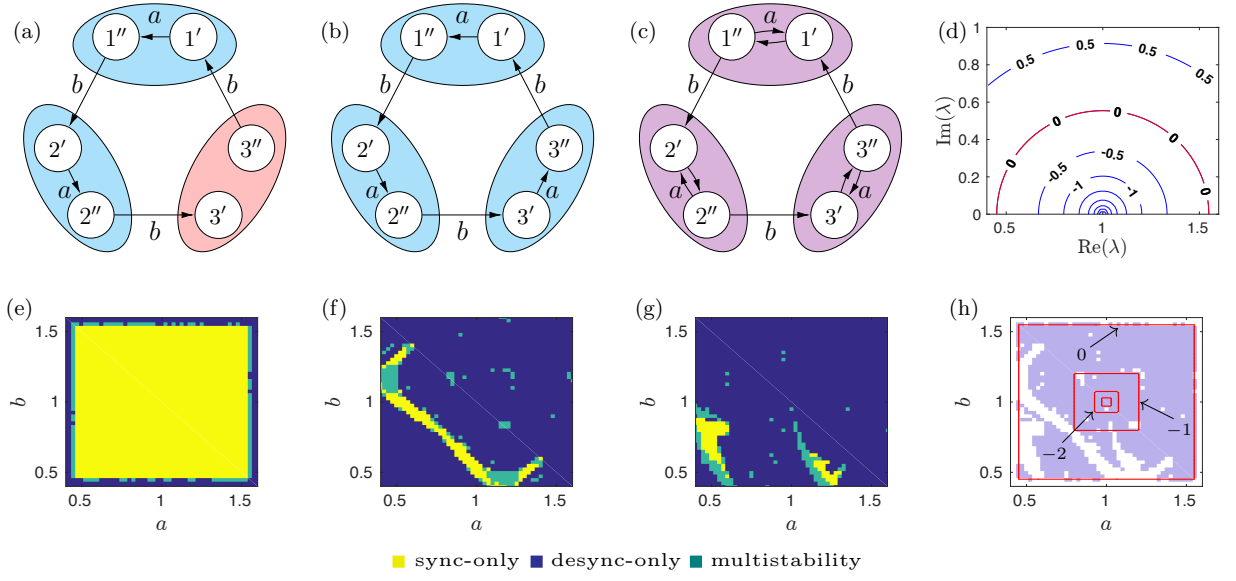


FIG. 4. Example of coupled electro-optic system showing *AISync*. (a–c) Networks with heterogeneous (a) and homogeneous nodes (b,c). (d) Stability function $\psi(\lambda)$ for the electro-optic system. (e–g) numerical results indicating where each system in (a–c) is synchronizable in the parameter space. Each pixel is categorized into three classes according to 24 independent simulations from random initial conditions (see text for details). (h) The *AISync* region (shaded purple), which is the union of yellow and green regions in (e) minus the analogous unions in (f) and (g). The red contours encode the MLE for the heterogeneous system.

in both directions). When the same choice is made for all internal connections, this leads to four different homogeneous systems, but two of them have $\lambda_2 = 0$ (not synchronizable), leaving only two homogeneous systems to consider [Figs. 4(b) and (c)]. For comparison, we take the heterogeneous system in Fig. 4(a), which forms a directed chain network in its monolayer representation. Each of the three systems [Figs. 4(a–c)] has a companion plot showing under what parameters the nodes are synchronizable [Figs. 4(e–g)]. In the latter panels, each pixel is generated from 24 independent simulations run from random initial conditions. The pixels are then color-coded according to how many times a fully synchronized state was reached after 2500 iterations (“sync-only”: 24 times; “desync-only”: 0 times; “multistability”: all other cases). Here we consider a trajectory to be fully synchronized if the synchronization error e defined in Eq. (D1) and averaged over the last 100 iterations falls below 10^{-3} . It is worth noting that, in this example, when a homogeneous system is synchronizable the synchronous state is always in the form of cluster synchronization among subnodes (those indexed with prime and double prime form two separate synchronized clusters), since complete synchronization among subnodes is always unstable for both homogeneous systems.

Figure 4(d) shows the stability function $\psi(\lambda)$ for the electro-optic subnode dynamics and coupling function, which has a bounded stable region. The lines are quite dense inside the stable region, meaning that the stability landscape is steep there and the function reaches very deep negative values. This is confirmed in Fig. 4(h),

where the *AISync* regions are shaded purple, with the MLE of the synchronous state for the heterogeneous system shown as red contour lines.

D. Other examples

The three *AISync* systems considered in this section include both linear and nonlinear coupling functions, as well as discrete- and continuous-time dynamics. While they provide *AISync* examples with directed network structures and bounded stability regions, we also demonstrate *AISync* for systems with unbounded stability region (SM Sec. S1), and for systems with undirected network structure (SM Sec. S2) [28].

VI. PROPENSITY FOR *AISync*

But how often does a network structure support *AISync*? To systematically address this question, we use the spread σ of the eigenvalues of the Laplacian matrix \tilde{L} for the monolayer network representation, which is a measure of synchronizability [8] defined by $\sigma^2 := \sum_{j=2}^n |\lambda_j - \bar{\lambda}|^2 / [d^2(n-1)]$, where $d := \sum_{j=1}^n \tilde{L}_{jj}/n$ and $\bar{\lambda} := \sum_{j=2}^n \lambda_j / (n-1)$. A smaller σ indicates higher synchronizability. Given an external sublink structure corresponding to a symmetric network, we compare the minimum spread σ_+ among all systems with homogeneous $F^{(i)}$ to the corresponding minimum σ_- among all

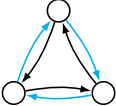
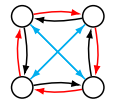
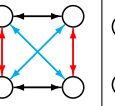
	$N = 3$	$N = 4$	$N = 5$
symmetric networks			
Q (optimal)	9	14	21
Q ($r > 0.2$)	11	81	254
Q ($r > 0.05$)	29	318	2154
B ($r > 0.2$)	11	101	204
B ($r > 0.05$)	31	400	2406

TABLE I. Number of isomorphically distinct *AISync*-favoring networks, listed for $N = 3, 4, 5$ nodes and $L = 2$ layers (with $a = b = 1$ to enable counting). The numbers are given for both binary (B) and quaternary (Q) choices of internal sublink configurations, as well as for different *AISync* strength (as measured by r defined in the text). The network diagrams encode all possible symmetric networks of a given size.

systems with strictly heterogeneous $F^{(i)}$. We call the structure *AISync-favoring* if $\sigma_{\neq} < \sigma_{=}$, which indicates that heterogeneous $F^{(i)}$ can make the system easier to synchronize than any homogeneous $F^{(i)}$. As a measure of how strongly the structure supports *AISync*, we define $r := 1 - \sigma_{\neq}/\sigma_{=} \leq 1$, where $r > 0$ indicates an *AISync*-favoring structure, and $r = 1$ implies $\sigma_{\neq} = 0$ (i.e., there is a heterogeneous system with optimal synchronizability). For example, the structure in Fig. 3 has $\sigma_{=} \approx 0.56$ and $\sigma_{\neq} \approx 0.33$, and $r \approx 0.41$.

Using this *AISync* strength r , we first enumerate all networks of a given size supporting *AISync* (Table I). For each N , we generate one or more diagrams representing all N -node symmetric networks, which are shown in the first row of Table I for $N = 3, 4, 5$. In these diagrams, each color indicates a set of links that, in any given symmetric network, must all exist together and be of the same type or not exist at all (noting that links from different sets can be of the same type). For example, there are three distinct symmetric networks for $N = 3$: a directed ring (cyan or black links), an undirected ring (cyan and black links of the same type), and the superposition of two directed rings in opposite directions (cyan and black links of different types; as in Fig. 3). For a given symmetric network derived from these diagrams, we choose the external sublink pattern for each link type from all possible ways of connecting a subnode pair to another. For the internal sublink patterns, we use either the binary or quaternary choices, where each node has one directed sublink (in either direction) in the binary case, while all four possibilities are allowed in the quaternary case. The rest of Table I lists the total numbers of isomorphically distinct external sublink structures \tilde{A} with $r > 0.05$, $r > 0.2$, and (optimal) $r = 1$; see Supplementary Table S1 and S2 for all optimal networks with $N = 3$ and 4.

Table II extends the first row in Table I, showing the symmetric network diagrams for $N = 6, 7$, and 8. In each

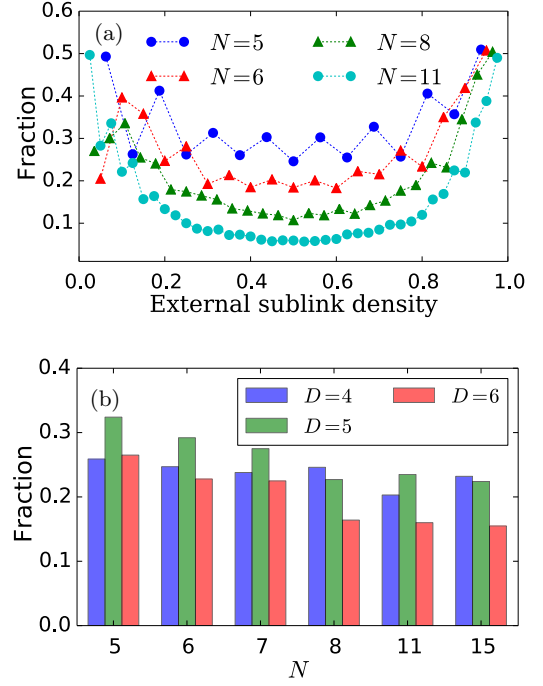
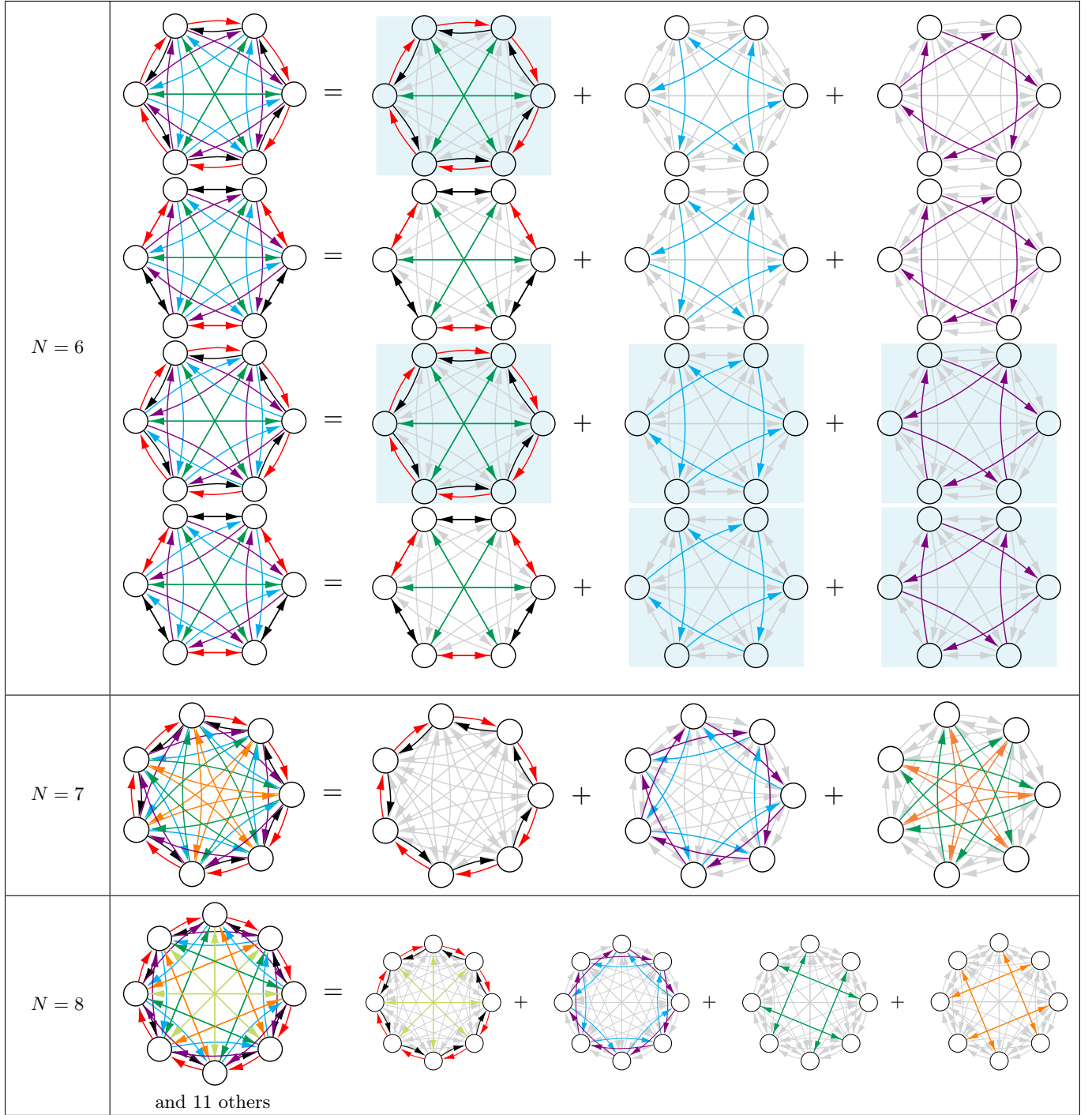


FIG. 5. Statistics on the prevalence of *AISync*-favoring networks. Shown as functions of (a) external sublink density and (b) network size N . Both panels show the fraction of systems with *AISync* strength $r > 0.05$ among those with circulant-graph network structures, where the external sublink density is given by $D/[L^2(N-1)]$, and D is the external sublink in-degree.

row, the leftmost diagram is the full representation as in Table I, which is decomposed into individual components (the other diagrams in the same row) to make them more clearly visible. The partial diagrams with the same background color indicate identical components appearing in multiple rows. Thus, for $N = 6$, we have four different diagrams (rows), each with a different combination of components. There is only one diagram for $N = 7$, while we show one representative diagram out of twelve in the case of $N = 8$.

Figure 5 shows the statistics of *AISync*-favoring networks. For numerical feasibility, we focus on those systems whose network structure is a directed, multi-link type, circulant graph (which covers all symmetric networks if N is prime). Sampling uniformly within this class, we observe that significant fraction of external sublink structures are *AISync*-favoring over a range of sublink densities [Fig. 5(a)] and network sizes [Fig. 5(b)]. We also observe that sparse and dense structures favor *AISync* more often than medium-density ones, despite the expectation that the effect of internal sublink heterogeneity would be smaller with higher external sublink density. This phenomenon is further explored in Appendix G by establishing the approximate left-right symmetry in Fig. 5(a).

TABLE II. Diagrams of symmetric networks with $N = 6, 7$, and 8 nodes.

VII. DISCUSSION

Given a symmetric network of identical oscillators, it is instructive to compare our results above in which the symmetry is broken by making the oscillators nonidentical with the alternative scenario in which the symmetry

is broken by making the network structure asymmetric. For directed unweighted networks of diffusively-coupled identical oscillators, it can be shown that: 1) with the exception of the complete graphs, all topologies that optimize synchronizability (i.e., those with $\sigma = 0$) are asymmetric [29]; 2) any network topology that can be spanned from a node (i.e., $\min_{i \geq 2} \text{Re}(\lambda_i) > 0$) embeds optimally

synchronizable subnetworks generated by deleting a subset of links [8, 30]. For example, a synchronous state that is not stable for a directed ring network may become stable for a directed chain formed by removing a link. More generally, introducing structural heterogeneity (breaking the symmetry of the network) can stabilize otherwise unstable homogeneous (symmetric) states.

Finally, we note that the defining characteristic of *AISync* considered here—that preserving the symmetry of a stable state requires breaking the symmetry of the system—can bear analogs in oscillator networks whose structure is not necessarily symmetric. Such a network can always be partitioned into symmetric subnetwork clusters (structurally equivalent subsets of nodes) that are candidates for cluster synchronization [16, 31, 32]. Synchronization of one of these clusters plays the role of complete synchronization in a symmetric network, which opens the possibility of exploiting *AISync* to tune cluster synchronization patterns through oscillator heterogeneity in arbitrary complex networks. We hope that our findings, and future theoretical and experimental studies they will stimulate, will significantly advance understanding of the interplay between symmetry and network dynamics.

ACKNOWLEDGMENTS

The authors thank Thomas Wytock and Young Sul Cho for insightful discussions. This work was supported by ARO Grant No. W911NF-15-1-0272.

Appendix A: Definition of Cayley graphs

Given a generating set S of a finite group G , the Cayley graph associated with S and G is defined as the network in which a node represents an element of G and a directed link from one node $g \in G$ to another $g' \in G$ represents the composition of some element $s \in S$ with g that gives g' (i.e., $gs = g'$). While such a network is generally directed, it will be undirected if the inverse of every element of S belongs to S . Choosing S to be a generating set guarantees that the resulting network is (strongly) connected. A generalization to multiple link types can be obtained if we assign different elements of S to different link types.

Appendix B: Details on multilayer models

Since Eq. (2) defines a subclass of systems governed by Eq. (1), it can always be written in the form of Eq. (1) for a given network structure specified by $A^{(\alpha)}$. This can be seen by stacking the m -dimensional vectors in Eq. (2)

and defining appropriate functions as follows:

$$\mathbf{X}_i := \begin{pmatrix} \mathbf{x}_1^{(i)} \\ \vdots \\ \mathbf{x}_L^{(i)} \end{pmatrix}, \quad \mathbf{F}_i := \begin{pmatrix} \mathbf{F}_1^{(i)} \\ \vdots \\ \mathbf{F}_L^{(i)} \end{pmatrix}, \quad \mathbf{H}^{(\alpha)} := \begin{pmatrix} \mathbf{H}_1^{(\alpha)} \\ \vdots \\ \mathbf{H}_L^{(\alpha)} \end{pmatrix}, \quad (\text{B1})$$

$$\mathbf{F}_\ell^{(i)}(\mathbf{X}_i) := \mathbf{f}(\mathbf{x}_\ell^{(i)}) + \sum_{\ell'=1}^L \tilde{A}_{\ell\ell'}^{(ii)} [\mathbf{h}(\mathbf{x}_{\ell'}^{(i)}) - \mathbf{h}(\mathbf{x}_\ell^{(i)})], \quad (\text{B2})$$

$$\mathbf{H}_\ell^{(\alpha)}(\mathbf{X}_i, \mathbf{X}_{i'}) := \sum_{\ell'=1}^L B_{\ell\ell'}^{(\alpha)} [\mathbf{h}(\mathbf{x}_{\ell'}^{(i')}) - \mathbf{h}(\mathbf{x}_\ell^{(i)})], \quad (\text{B3})$$

where $B_{\ell\ell'}^{(\alpha)}$ is the value of $\tilde{A}_{\ell\ell'}^{(ii')}$ when nodes i' is connected to node i by a link of type α . Thus, in the adjacency matrix \tilde{A} , each size- L off-diagonal block equals one of the matrices $B^{(\alpha)} = (B_{\ell\ell'}^{(\alpha)})$, and the arrangement of those blocks that equals $B^{(\alpha)}$ reflects the topology of node-to-node interactions through links of type α , represented by the adjacency matrix $A^{(\alpha)}$ (see Fig. 1(d) for an example). Note that these node-to-node interactions are not necessarily diffusive, since we can have $\mathbf{H}^{(\alpha)}(\mathbf{X}_i, \mathbf{X}_{i'}) \neq \mathbf{0}$ even for $\mathbf{X}_i = \mathbf{X}_{i'}$, if $\mathbf{x}_\ell^{(i)} \neq \mathbf{x}_{\ell'}^{(i')}$ for some $\ell \neq \ell'$ [which in particular means that the coupling term cannot be written in the form $\mathbf{H}^{(\alpha)}(\mathbf{X}_i, \mathbf{X}_{i'}) = \tilde{\mathbf{H}}^{(\alpha)}(\mathbf{X}_{i'}) - \tilde{\mathbf{H}}^{(\alpha)}(\mathbf{X}_i)$]. For example, even when nodes 1 and 4 are synchronized in the network of Fig. 1, i.e., $\mathbf{X}_1 = \mathbf{X}_4 = (\mathbf{s}_1(t), \mathbf{s}_2(t))^T$, the coupling term corresponding to the link of type $\alpha = 3$ between them is in general not identically zero:

$$\mathbf{H}^{(3)}(\mathbf{X}_1, \mathbf{X}_4) = \begin{pmatrix} \mathbf{h}(\mathbf{s}_2) - \mathbf{h}(\mathbf{s}_1) \\ 0 \end{pmatrix} \neq \mathbf{0}. \quad (\text{B4})$$

However, since we assume identical dynamics for subnodes and diffusive coupling between subnodes, a synchronous state of Eq. (2) given by $\mathbf{x}_\ell^{(i)}(t) = \mathbf{s}(t)$, $\forall i, \ell$ with $\dot{\mathbf{s}} = \mathbf{f}(\mathbf{s})$ is guaranteed to exist even if $\mathbf{F}^{(i)}$'s are heterogeneous. This corresponds to a global synchronous state of Eq. (1) defined by $\mathbf{X}_i = \mathbf{S} := (\mathbf{s}, \dots, \mathbf{s})^T$, $\forall i$, which can be verified by noting that $\mathbf{H}^{(\alpha)}(\mathbf{S}, \mathbf{S}) = \mathbf{0}$ and $\mathbf{F}_\ell^{(i)}(\mathbf{S}) := \mathbf{f}(\mathbf{s})$, $\forall i$.

Appendix C: Details on MSF analysis

Equation (2) can be rewritten as a monolayer network by defining a single index for all the $n := LN$ subnodes, in which node i has subnodes $j = k_{i1}, \dots, k_{iL}$ with $k_{i\ell} := (i-1)L + \ell$. This leads to the standard form for a (monolayer) diffusively coupled network of oscillators:

$$\dot{\mathbf{x}}_j = \mathbf{f}(\mathbf{x}_j) + \sum_{j'=1}^n \tilde{A}_{jj'} [\mathbf{h}(\mathbf{x}_{j'}) - \mathbf{h}(\mathbf{x}_j)], \quad (\text{C1})$$

where $\mathbf{x}_j = \mathbf{x}_\ell^{(i)}$ and $\tilde{A}_{jj'} := \tilde{A}_{\ell\ell'}^{(ii')}$ for $j = k_{i\ell}$ and $j' = k_{i'\ell'}$. This equation allows application of the MSF analysis [25] because subnodes and sublinks (and the associated interaction functions) are identical. The stability function $\psi(\lambda)$ is defined as the maximum Lyapunov exponent of the reduced variational equation,

$$\dot{\boldsymbol{\xi}} = [D\mathbf{f}(\mathbf{s}) - \lambda D\mathbf{h}(\mathbf{s})]\boldsymbol{\xi}, \quad (\text{C2})$$

where $\boldsymbol{\xi}$ is an m -dimensional perturbation vector, $D\mathbf{f}(\mathbf{s})$ and $D\mathbf{h}(\mathbf{s})$ are the Jacobian of \mathbf{f} and \mathbf{h} , respectively, at the synchronous state, $\mathbf{x}_j = \mathbf{s}(t)$, $\forall j$, and λ is a complex-valued parameter.

Appendix D: Verifying the *AISync* conditions

Here we describe our scheme for verifying *AISync* conditions (C1) and (C2) given a symmetric network structure (adjacency matrix $A^{(\alpha)}$), external sublink configurations (matrices $B^{(\alpha)}$), a set \mathcal{F} of possible internal sublink configurations (from which matrices $F^{(i)}$ are chosen), isolated subnode dynamics (\mathbf{f}), and coupling function for sublinks (\mathbf{h}). We first obtain the stability function $\psi(\lambda)$:

1. Compute a trajectory $\mathbf{s}(t)$ of an isolated subnode by integrating $\dot{\mathbf{s}} = \mathbf{f}(\mathbf{s})$, which determines the synchronous state, $\mathbf{x}_\ell^{(i)}(t) = \mathbf{s}(t)$, $\forall i, \ell$.
2. Integrate Eq. (C2) and calculate its MLE, which defines $\psi(\lambda)$ for a range of λ in the complex plane.

Note that $\psi(\lambda)$ depends only on \mathbf{f} , \mathbf{h} , and $\mathbf{s}(t)$. For a given symmetric network structure and external sublink configurations, we can compute the stability Ψ of the synchronous state for any combination of $F^{(i)} \in \mathcal{F}$ by calculating and substituting the Laplacian eigenvalues λ_j into the formula $\Psi = \max_{2 \leq j \leq n} \psi(\lambda_j)$. To establish the *AISync* property, we verify the following conditions:

- (C1)': For each matrix $F \in \mathcal{F}$, set $F^{(1)} = \dots = F^{(N)} = F$ (leading to a homogeneous system) and verify $\Psi > 0$.
- (C2)': Identify a combination of (heterogeneous) $F^{(i)} \in \mathcal{F}$ for which $\Psi < 0$ (e.g., by checking exhaustively or by using a numerical optimization algorithm to minimize Ψ over $F^{(i)}$).

The verification of condition (C1)' provides strong support for (C1), since the only other possibility for a stable synchronization of all nodes is a state of the form $\mathbf{x}_\ell^{(i)} = \mathbf{s}_\ell(t)$, $\forall i, \ell$, with at least one $\mathbf{s}_\ell(t)$ different from the others (which we find does not exist in many cases, such as the examples in Fig. 3 and in SM Sec. 1). To provide additional support for (C1), we directly simulate Eq. (2) from a set of initial conditions and verify that the synchronization error e does not approach zero whenever

$F^{(1)} = \dots = F^{(N)}$, where e is defined as the standard deviation of the node state vectors, or equivalently,

$$e^2 := \frac{1}{N} \sum_{i=1}^N \sum_{\ell=1}^L \|\mathbf{x}_\ell^{(i)} - \bar{\mathbf{x}}_\ell\|^2, \quad \bar{\mathbf{x}}_\ell := \frac{1}{N} \sum_{i=1}^N \mathbf{x}_\ell^{(i)}. \quad (\text{D1})$$

Here $\|\cdot\|$ denotes the 2-norm in the state space of the subnode dynamics and $e = 0$ is achieved if and only if the system is in a synchronous state of the form $\mathbf{x}_\ell^{(i)} = \mathbf{s}_\ell(t)$. To complete our procedure, we verify condition (C2)', which rigorously establishes (C2).

Appendix E: Details on example in Fig. 2

In the example system from Fig. 3, the coupling matrix $\tilde{A}^{(ii')}$ for external sublinks is set to $\begin{pmatrix} b & b \\ 0 & 0 \end{pmatrix}$ or $\begin{pmatrix} 0 & 0 \\ 0 & b \end{pmatrix}$, corresponding to the two types of links, where the constant b represents the coupling strength common to all external sublinks. The coupling matrix $F^{(i)}$ for internal sublinks is chosen from the binary set $\mathcal{F} = \{\begin{pmatrix} 0 & a \\ 0 & 0 \end{pmatrix}, \begin{pmatrix} 0 & 0 \\ a & 0 \end{pmatrix}\}$, corresponding to the two possible sublink directions [and thus to two types of nodes indicated by green and cyan color, respectively, in Fig. 3(a)], where the constant a represents the coupling strength common to all internal sublinks. The Lorenz dynamics of the subnodes and the coupling represented by sublinks are given by

$$\begin{aligned} \mathbf{f}(\mathbf{x}) &= \begin{pmatrix} \gamma(x_2 - x_1) \\ x_1(\rho - x_3) - x_2 \\ x_1x_2 - \beta x_3 \end{pmatrix}, \\ \mathbf{h}(\mathbf{x}) &= \begin{pmatrix} x_2 \\ 0 \\ 0 \end{pmatrix}, \quad \mathbf{x} = \begin{pmatrix} x_1 \\ x_2 \\ x_3 \end{pmatrix} \end{aligned} \quad (\text{E1})$$

with the standard parameters, $\gamma = 10$, $\rho = 28$, and $\beta = 8/3$.

The stability function $\psi(\lambda)$ is determined by Eq. (C2), which for this system reads

$$\begin{pmatrix} \dot{\xi}_1 \\ \dot{\xi}_2 \\ \dot{\xi}_3 \end{pmatrix} = \begin{pmatrix} -\gamma & \gamma - \lambda & 0 \\ \rho - s_3 & -1 & -s_1 \\ s_2 & s_1 & -\beta \end{pmatrix} \begin{pmatrix} \xi_1 \\ \xi_2 \\ \xi_3 \end{pmatrix}, \quad (\text{E2})$$

where $\boldsymbol{\xi} := (\xi_1, \xi_2, \xi_3)^T$ is the variation of the state vector \mathbf{x} and the synchronous state $\mathbf{s} := (s_1, s_2, s_3)^T$ satisfies the equation for a single isolated Lorenz oscillator:

$$\begin{aligned} \dot{s}_1 &= \gamma(s_2 - s_1), \\ \dot{s}_2 &= s(\rho - s_3) - s_2, \\ \dot{s}_3 &= s_1s_2 - \beta s_3. \end{aligned} \quad (\text{E3})$$

For a given λ in the complex plane, we compute $\psi(\lambda)$ by numerically integrating Eqs. (E2) and (E3) for 2×10^4 time units and estimating the MLE [33] associated with the variable $\boldsymbol{\xi}$. Figure 6 shows the resulting estimate of $\psi(\lambda)$, which has a bounded stability region $\{\lambda \in \mathbb{C} \mid \psi(\lambda) < 0\}$.

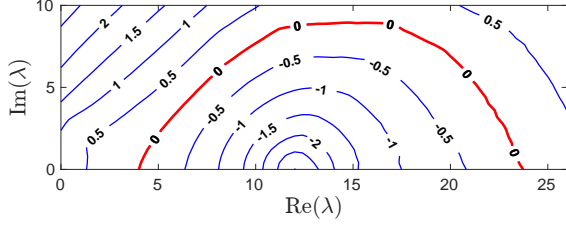


FIG. 6. Stability function $\psi(\lambda)$ for the *AISync* system in Fig. 3.

For a given combination of a and b , we obtain Ψ_+ and Ψ_- , which are shown in Fig. 3(b). Note that for this example there are only two distinct homogeneous systems and two distinct heterogeneous systems. One of these heterogeneous systems is shown in Fig. 3(a). We also note that $\Psi_+ > 0$ and $\Psi_- < 0$ are equivalent to the conditions (C1)' and (C2)' in Sec. D, respectively. For each combination of a and b satisfying both conditions [on a grid covering Fig. 3(b) with a resolution of 0.2], we additionally run 24 direct simulations of Eq. (2) for 200 time units. The initial condition $\mathbf{x}_\ell^{(i)}(0)$ for each subnode is chosen randomly and independently from the uniform distribution in the region $[0, 10] \times [0, 10] \times [0, 10]$ of its state space. The results confirm that the synchronization error e defined in Eq. (D1) and averaged over the last 100 iterations does not fall below 10^{-3} in all 24 runs for both homogeneous systems, providing solid evidence that the system satisfies the *AISync* condition (C1) for these combinations of a and b . Since $\Psi_- < 0$ implies (C2)' and thus (C2), this confirms *AISync* in the region shaded purple in Fig. 3(b).

The initial condition for the sample trajectory in Fig. 3(c) is chosen randomly within a distance of 10^{-3} from the synchronous state. The trajectory is then computed by integrating the system with all nodes green for $t \leq 25$, instantaneously switching the direction of the sublink between subnodes 2' and 2'', and then continuing to integrate for $25 \leq t \leq 50$.

Appendix F: Sampling protocol used in Fig. 4

We randomly sample systems whose network structure $A^{(\alpha)}$ is a circulant graph (with directed links of possibly multiple types) of given size N and external sublink in-degree D (i.e., the total number of sublinks connected to the subnodes of a given node). Each of the D sublinks coming into node 1 is chosen randomly; it connects a random subnode chosen uniformly from the other $N - 1$ nodes to a random subnode chosen uniformly from node 1. The incoming sublinks into nodes 2 to N are then chosen to precisely match those coming into node 1, which ensures that the network structure is a circulant graph. This simultaneously specifies $A^{(\alpha)}$ and $B^{(\alpha)}$ defining the system. To determine σ_\neq , σ_+ , and r for this system, we

calculate the eigenspread σ of the monolayer network representation for all the possible internal sublink configurations $F^{(i)}$, chosen here from the binary set $\{(\begin{smallmatrix} 0 & 1 \\ 0 & 0 \end{smallmatrix}), (\begin{smallmatrix} 0 & 0 \\ 1 & 0 \end{smallmatrix})\}$. For each combination of N and D , we generate a sample of 4,000 such systems to compute the fraction of *AISync* systems.

Appendix G: Approximate symmetry in Fig. 4(a)

The approximate symmetry with respect to the vertical line at density 0.5 observed in Fig. 4(a) can be explained using the notion of network complement. The complement of a given (unweighted) network with adjacency matrix $\tilde{A} = (\tilde{A}_{jj'})$ is defined as the network having the adjacency matrix $\tilde{A}^c = (\tilde{A}_{jj'}^c)$ given by

$$\tilde{A}_{jj'}^c := (1 - \tilde{A}_{jj'})(1 - \delta_{jj'}). \quad (\text{G1})$$

The external sublink density of a network and its complement add up to one, placing them symmetrically about the vertical line at density 0.5 in Fig. 4(a). When the nontrivial Laplacian eigenvalues of the network and its complement, which we denote $\lambda_2, \dots, \lambda_n$ and $\lambda_2^c, \dots, \lambda_n^c$, respectively, are both indexed in the order of increasing real part, they are related by $\lambda_j + \lambda_{n+2-j}^c = n$ [8]. This implies that, if σ is the eigenvalue spread for a monolayer network with given internal sublink configurations $F^{(i)}$, then the spread for its complement is given by

$$\sigma^c = \frac{\tilde{m}\sigma}{n(n-1) - \tilde{m}}, \quad (\text{G2})$$

where $\tilde{m} := \sum_j \sum_{j' \neq j} \tilde{A}_{jj'}$ is the number of directed links in the network \tilde{A} . Now consider two systems with n subnodes and adjacency matrices \tilde{A}_1 and \tilde{A}_2 , whose σ values are σ_1 and σ_2 , respectively. If we denote the σ values of the complement of these systems by σ_1^c and σ_2^c , respectively, we have

$$\frac{\sigma_1}{\sigma_2} = \frac{\sigma_1^c}{\sigma_2^c} \quad (\text{G3})$$

when \tilde{A}_1 and \tilde{A}_2 have the same number of directed links, i.e., $\tilde{m}_1 = \tilde{m}_2$. It follows from Eq. (G2) that if \tilde{A}_1 is the best homogeneous system and \tilde{A}_2 the best heterogeneous system for a given external connection pattern with density x , then their complements are the best homogeneous and heterogeneous system for an external connection pattern with density $1 - x$. Thus, the value of *AISync* strength r is the same at density x and $1 - x$. The symmetry, however, is not perfect between sparse and dense parts of the plot, since we exclude the cases in which the network is not synchronizable (i.e., $\min_{j \geq 2} \text{Re}(\lambda_j) > 0$), the effect of which is not symmetric between sparse and dense cases.

-
- [1] Juan G Restrepo, Edward Ott, and Brian R Hunt, “Spatial patterns of desynchronization bursts in networks,” *Phys. Rev. E* **69**, 066215 (2004).
- [2] Jie Sun, Erik M Bollt, and Takashi Nishikawa, “Master stability functions for coupled nearly identical dynamical systems,” *Europhys. Lett.* **85**, 60011 (2009).
- [3] Takashi Nishikawa, Adilson E Motter, Ying-Cheng Lai, and Frank C Hoppensteadt, “Heterogeneity in oscillator networks: Are smaller worlds easier to synchronize?” *Phys. Rev. Lett.* **91**, 014101 (2003).
- [4] Michael Denker, Marc Timme, Markus Diesmann, Fred Wolf, and Theo Geisel, “Breaking synchrony by heterogeneity in complex networks,” *Phys. Rev. Lett.* **92**, 074103 (2004).
- [5] Luca Donetti, Pablo I Hurtado, and Miguel A Munoz, “Entangled networks, synchronization, and optimal network topology,” *Phys. Rev. Lett.* **95**, 188701 (2005).
- [6] Adilson E Motter, Changsong Zhou, and Jürgen Kurths, “Network synchronization, diffusion, and the paradox of heterogeneity,” *Phys. Rev. E* **71**, 016116 (2005).
- [7] Changsong Zhou and Jürgen Kurths, “Dynamical weights and enhanced synchronization in adaptive complex networks,” *Phys. Rev. Lett.* **96**, 164102 (2006).
- [8] Takashi Nishikawa and Adilson E Motter, “Network synchronization landscape reveals compensatory structures, quantization, and the positive effect of negative interactions,” *Proc. Natl. Acad. Sci. U.S.A.* **107**, 10342–10347 (2010).
- [9] Takashi Nishikawa and Adilson E. Motter, “Symmetric states requiring system asymmetry,” *Phys. Rev. Lett.* **117**, 114101 (2016).
- [10] Yoshiki Kuramoto and Dorjsuren Battogtokh, “Coexistence of coherence and incoherence in nonlocally coupled phase oscillators,” *Nonlinear Phenom. Complex Syst.* **5**, 380 (2002).
- [11] Daniel M Abrams and Steven H Strogatz, “Chimera states for coupled oscillators,” *Phys. Rev. Lett.* **93**, 174102 (2004).
- [12] Norman Biggs, *Algebraic graph theory* (Cambridge university press, 1993).
- [13] Mark J Panaggio and Daniel M Abrams, “Chimera states: coexistence of coherence and incoherence in networks of coupled oscillators,” *Nonlinearity* **28**, R67 (2015).
- [14] The On-Line Encyclopedia of Integer Sequences, published electronically at <https://oeis.org>, 2007, Sequence A006799.
- [15] Thomas Dahms, Judith Lehnert, and Eckehard Schöll, “Cluster and group synchronization in delay-coupled networks,” *Phys. Rev. E* **86**, 016202 (2012).
- [16] Louis M Pecora, Francesco Sorrentino, Aaron M Hagerstrom, Thomas E Murphy, and Rajarshi Roy, “Cluster synchronization and isolated desynchronization in complex networks with symmetries,” *Nat. Commun.* **5** (2014).
- [17] Charo I. del Genio, Jesús Gómez-Gardeñes, Ivan Bonamassa, and Stefano Boccaletti, “Synchronization in networks with multiple interaction layers,” *Sci. Adv.* **2** (2016).
- [18] Jianxi Gao, Sergey V Buldyrev, H Eugene Stanley, and Shlomo Havlin, “Networks formed from interdependent networks,” *Nature Phys.* **8**, 40–48 (2012).
- [19] Sergio Gomez, Albert Diaz-Guilera, Jesus Gomez-Gardeñes, Conrad J Perez-Vicente, Yamir Moreno, and Alex Arenas, “Diffusion dynamics on multiplex networks,” *Phys. Rev. Lett.* **110**, 028701 (2013).
- [20] Manlio De Domenico, Albert Solé-Ribalta, Emanuele Cozzo, Mikko Kivelä, Yamir Moreno, Mason A Porter, Sergio Gómez, and Alex Arenas, “Mathematical formulation of multilayer networks,” *Phys. Rev. X* **3**, 041022 (2013).
- [21] Stefano Boccaletti, Ginestra Bianconi, Regino Criado, Charo I Del Genio, Jesús Gómez-Gardeñes, Miguel Romance, Irene Sendiña-Nadal, Zhen Wang, and Massimiliano Zanin, “The structure and dynamics of multilayer networks,” *Phys. Rep.* **544**, 1–122 (2014).
- [22] Manlio De Domenico, Clara Granell, Mason A Porter, and Alex Arenas, “The physics of spreading processes in multilayer networks,” *Nature Phys.* **12**, 901–906 (2016).
- [23] Xiyun Zhang, Stefano Boccaletti, Shuguang Guan, and Zonghua Liu, “Explosive synchronization in adaptive and multilayer networks,” *Phys. Rev. Lett.* **114**, 038701 (2015).
- [24] Lucia Valentina Gambuzza, Mattia Frasca, and Jesus Gomez-Gardeñes, “Intra-layer synchronization in multiplex networks,” *Europhys. Lett.* **110**, 20010 (2015).
- [25] Louis M Pecora and Thomas L Carroll, “Master stability functions for synchronized coupled systems,” *Phys. Rev. Lett.* **80**, 2109 (1998).
- [26] Zhongkui Li, Zhisheng Duan, Guanrong Chen, and Lin Huang, “Consensus of multiagent systems and synchronization of complex networks: a unified viewpoint,” *IEEE Trans. Circuits Syst. I, Reg. Papers* **57**, 213–224 (2010).
- [27] Aaron M Hagerstrom, Thomas E Murphy, Rajarshi Roy, Philipp Hövel, Iryna Omelchenko, and Eckehard Schöll, “Experimental observation of chimeras in coupled-map lattices,” *Nature Phys.* **8**, 658–661 (2012).
- [28] See Supplemental Material at [URL] for Supplementary Tables and more systems showing AISync.
- [29] For an N -node directed unweighted network, the total number of links \tilde{m} must be divisible by $N - 1$ if the network is optimal [8], while \tilde{m} must be divisible by N if the network is homogeneous, which requires the in- and out-degrees of all nodes to be equal. Since $\tilde{m} \leq N(N - 1)$, the two divisibility conditions can be satisfied only if $\tilde{m} = N(N - 1)$ (i.e., if the network is a complete graph).
- [30] Takashi Nishikawa and Adilson E Motter, “Synchronization is optimal in nondiagonalizable networks,” *Phys. Rev. E* **73**, 065106 (2006).
- [31] Martin Golubitsky and Ian Stewart, “Rigid patterns of synchrony for equilibria and periodic cycles in network dynamics,” *Chaos* **26**, 094803 (2016).
- [32] Vincenzo Nicosia, Miguel Valencia, Mario Chavez, Albert Díaz-Guilera, and Vito Latora, “Remote synchronization reveals network symmetries and functional modules,” *Phys. Rev. Lett.* **110**, 174102 (2013).
- [33] Alan Wolf, Jack B Swift, Harry L Swinney, and John A Vastano, “Determining lyapunov exponents from a time series,” *Physica D* **16**, 285–317 (1985).